agriculture

MDPI

Article

Dynamics of Energy Fluxes in a Mediterranean Vineyard: Influence of Soil Moisture

Ricardo Egipto [1,*], Arturo Aquino [2] and José Manuel Andújar [2]

[1] INIAV, I.P.—Instituto Nacional de Investigação Agrária e Veterinária, Pólo de Inovação de Dois Portos, Quinta da Almoínha, 2565-191 Dois Portos, Portugal
[2] CITES, Centro de Investigación en Tecnología, Energía y Sostenibilidad, Universidad de Huelva, La Rábida, Palos de la Frontera, 21819 Huelva, Spain; arturo.aquino@diesia.uhu.es (A.A.); andujar@uhu.es (J.M.A.)
* Correspondence: ricardo.egipto@iniav.pt

Abstract: Accurate evaluation of grapevine water use is essential for optimizing water management and maximizing grapevine yield and berry quality in Mediterranean climates. Understanding the water and heat flux dynamics in a vineyard during grapevine berry maturation is of utmost importance. This study focuses on evaluating sensible and latent energy fluxes at the canopy, the soil beneath the canopy, and the interrow areas. The primary objective is to develop a model framework for accurately estimating these energy fluxes, contributing to a better understanding of their behavior during berry ripening. The model's accuracy was assessed by comparing the estimated fluxes with those measured by an eddy-covariance system installed at a reference height of three meters in the experimental vineyard. This validation step was essential to confirm the model's ability to capture the intricate energy flux dynamics of the vineyard, especially during grape maturation. The results revealed a high level of agreement between the observed and estimated fluxes, confirming the model's reliability. This comprehensive evaluation of energy fluxes provides valuable insights for optimizing irrigation strategies. By doing so, this study contributes to improving grape quality, ensuring sustainable water resource use, and ultimately enhancing vineyard productivity in arid and water-scarce regions.

Keywords: vineyard; grapevine water use; radiative fluxes; turbulent fluxes

Citation: Egipto, R.; Aquino, A.; Andújar, J.M. Dynamics of Energy Fluxes in a Mediterranean Vineyard: Influence of Soil Moisture. *Agriculture* **2024**, *14*, 1845. https://doi.org/10.3390/agriculture14101845

Academic Editor: Tommaso Frioni

Received: 11 September 2024
Revised: 14 October 2024
Accepted: 16 October 2024
Published: 19 October 2024

1. Introduction

Mediterranean climates, characterized by mild winters, autumn-spring rainfall with erratic distribution, and recurrent drought in late spring and summer, are particularly favorable for viticulture [1,2]. These climatic conditions contribute significantly to global wine production, with some of the oldest and most prestigious wine-producing regions, such as Southern France, Italy, Spain, Portugal, and parts of Greece, located within the Mediterranean zone. Furthermore, regions like California, Chile, South Africa, and the southern coastal zone of Australia, which also experience Mediterranean climates, have gained recognition for producing high-quality wines that often rival those from traditional Mediterranean areas.

Mediterranean vineyards benefit from abundant sunlight, essential for grape ripening and flavor development [3]. However, excessive solar radiation can pose challenges, including heat and water stress [4–7]. Future climate projections indicate an increase in extreme weather events [8], with more frequent and intense occurrences of warmer, drier conditions and severe heatwaves with accompanying droughts expected in the near future [8–11]. Additionally, vineyards are typically planted in sparsely spaced rows and utilize drip irrigation, minimizing the wetted area to reduce soil water evaporation and optimize plant water use. Consequently, the exposed soil between vine rows (interrow) can act as a significant sink and/or source of energy [12–16]. Furthermore, in Mediterranean conditions, the absence of rain during grape ripening renders interrow soil evaporation

negligible compared to row soil evaporation and grapevine transpiration (T) in drip-irrigated vineyards. Under these circumstances, with a fully developed canopy, grapevine transpiration dominates the evapotranspiration (ET) process [17]. The partitioning between T and ET is strongly influenced by factors such as the grapevine leaf area index (LAI) and the area of soil covered by the projected canopy shade at midday (the fractional cover of the canopy, f) [12,18].

Convective energy fluxes (comprising sensible heat and latent heat fluxes) within the vineyard are directly influenced by the distribution of available radiative energy fluxes, which partition between the canopy and the soil surface [17,18]. A thorough understanding of energy partitioning and respective energy fluxes within the vineyard is crucial for adapting vineyard management to environmental conditions. To this end, several models have been developed to assess the energy balance in agricultural systems (see Table 1).

Table 1. Models for assessing energy balance in agricultural systems.

Model	General Description	References
Penman–Monteith (PM)	A big-leaf model conceptualizing the vegetation as a large, homogeneous, and uniformly saturated surface subjected to resistance to latent heat transfer. Furthermore, it postulates the equality between the aerodynamic resistances for sensible and latent heat transfer to the atmosphere.	[19]
Shuttleworth and Wallace (S-W)	A one-dimensional model describing the energy partition in sparse crops. The analytical approach utilizes two Penman–Monteith equations: one applied to the crop and another to the soil surface.	[20]
Two-source energy balance (TSEB)	A two-source model of energy fluxes incorporating the view geometry associated with directional radiometric surface temperature measurement.	[21]
Clumped model	A two-source model adapted to a semi-arid shrubland incorporating vegetation clumping as defined by the fractional vegetative cover to estimate energy fluxes from both soil (beneath vegetation and bare soil) and shrubs.	[16]
Three-source energy balance (3SEB)	An adaptation of the TSEB model to enhance the partitioning of latent energy fluxes from heterogeneous and sparse canopies.	[12,15]

Vineyards, characterized by widely spaced rows, 2 to 3 m apart, and vertical shoot positioning systems, result in a unique energy balance system. The concentration of foliage in the upper two-thirds of the vine canopy leaves significant soil surface area exposed, making energy fluxes at both interrow and under-vine soil crucial to the vineyard's overall energy dynamics [17,18,22]. This exposed soil experiences increased radiation and evaporative demand, influencing vertical temperature profiles within the canopy [4,13,18]. Additionally, the small-wetted area characteristic of drip irrigation systems promotes thermal convection while minimizing evaporation [23,24], resulting in a greater proportion of sensible heat directed towards both the canopy and soil [4,13,23,24].

These factors necessitate tailoring energy balance models to accurately capture the complexities of vineyard systems, including turbulent energy fluxes from the soil between rows, the soil beneath the canopy, and the vine canopy itself. The three-source clumped model is particularly suited to systems, like vineyards, with significant spatial variability due to row structure and vertical development of the canopy. This model must comprehensively account for energy fluxes and resistances from all components: vegetation, bare or cover-cropped soil between rows, and bare soil under the vines. As radiation transmission to the surface through interrow spaces, canopy gaps, and canopy leaves, fluctuate throughout the day, the model must also reliably describe radiation divergence through the canopy [18].

This article investigates the dynamics of energy fluxes in a drip-irrigated vineyard under regulated deficit irrigation in an arid climate during the 2021 grape maturation period. A novel framework, based on the three-source clumped model initially developed by Brenner and Incoll [16] and further developed by Lhomme et al. [15], is introduced to provide insights into the distribution of available energy and to calculate energy fluxes within the vineyard. The framework allows for the independent measurement of heat fluxes from each vineyard component—the vine canopy, bare soil between rows, and bare soil beneath the vines. Additionally, latent energy fluxes from each component are estimated as the unknowns to their respective energy balance equations.

This research aims to enhance our understanding of energy dynamics in vineyards under regulated deficit irrigation, providing valuable insights for optimizing irrigation management and grape production in arid climates.

2. Materials and Methods

2.1. Location and Experimental Layout

This experiment was carried out during the 2021 growing season at Herdade do Esporão, a commercial vineyard located in Reguengos de Monsaraz, in the Alentejo wine region of southern Portugal (lat. 38°23′55″ N; long. 7°32′46″ W). This study focused on a 17-year-old vineyard of the red *Vitis vinifera* cv. Tempranillo (syn. Aragonez), grafted onto 1103 Paulsen rootstock. The vines were planted in north-south rows, 3.0 m apart, with 1.5 m between vines within each row (resulting in a density of 2220 vines/ha). The vines were spur-pruned on a bilateral Royat cordon system, with each vine evenly pruned to 15–16 buds and trained to vertical shoot positioning. The soil, classified as a eutric cambisol with a silty-clay texture, had an average bulk density of 1.35 g.cm^{-3}, low organic matter content, an effective root depth of 1.0 m, and a pH range of 7.0 to 7.6. The average volumetric soil water content at field capacity (θ_{fc}) and wilting point (θ_{wp}) were 0.37 and 0.23 m^3.m^{-3}, respectively. Standard regional viticultural practices were followed, including maintaining bare soil under the vines and cultivating a native cover crop between rows. To minimize competition with the vines, the cover crop was sustained until mid-June and then allowed to dry out, leaving bare soil between the rows. Drip irrigation, using 2.4 L.h^{-1} emitters spaced 1.0 m apart, was applied weekly, in line with the vineyard owner's practices.

The field trial for studying vineyard energy fluxes, detailed in Section 2.4, was conducted during the ripening period of 2021, from 8 July to 31 August. Four days of intensive measurements—15 July, as well as 10, 18, and 26 August—are detailed in this work. For this purpose, ten healthy adult vines were randomly selected from two adjacent rows (five vines per row). This narrow selection criterion aimed to enhance measurement coherence and optimize data acquisition under conditions of low temporal and spatial variability. The experimental design also allowed for the assessment of solar radiation effects, as both sides of the canopy (east and west) were studied under contrasting incident radiation levels.

2.2. Climate Characterization

The study area experiences a Mediterranean climate, characterized by hot, dry summers and mild, rainy winters. From October 2020 to August 2021, the total rainfall recorded was 548.6 mm. Notably, no rainfall events occurred during the measurement days detailed in this study. The last rain event took place from 17 June to 20 June, resulting in an accumulated rainfall of 13.4 mm, which was also the total rainfall for June 2021 (Figure S1). Hourly averaged air temperature (*Tair*, °C) and air vapor pressure deficit (*VPD*, kPa), measured at the experimental plot during the experimental period, are shown in Figure 1. All measurements were taken under clear-sky conditions. Air temperature ranged from a minimum of 15.5 °C at sunrise to a maximum of 37.5 °C at 4 pm. *VPD* increased from a minimum of 0.15 kPa at sunrise to a maximum of 5.6 kPa at 4 pm. In the afternoon, air temperature consistently exceeded 33.5 °C, and the *VPD* remained above 4 kPa, before

both gradually declined later in the day. During the measurement period, the vineyard was irrigated on 11, 16, 23, and 29 of July, as well as on 1, 5, 8, 13, 22, and 26 August (Figure S1).

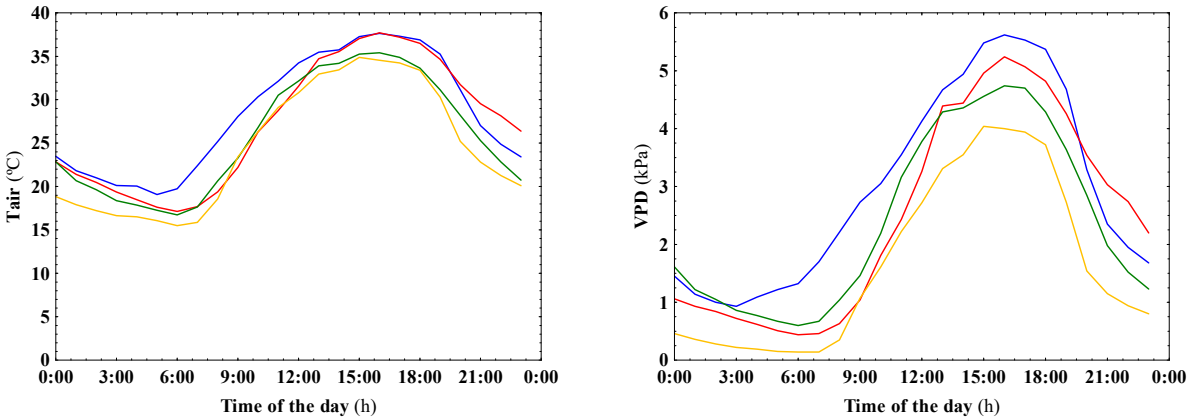

Figure 1. Atmospheric patterns on the measurement days. The figure illustrates the measurements of air temperature (*Tair*, °C) and air vapor pressure deficit (*VPD*, kPa) measured on 15 July (blue) and 10 (red), 18 (green), and 26 August 2021 (yellow) at the experimental plot.

2.3. Theoretical Background and Implemented Model Framework

Energy balance models are valuable tools for understanding how available radiative energy is partitioned into sensible and latent heat fluxes within a system. The Shuttleworth and Wallace model is considered suitable for assessing the crop energy balance in dense, homogeneous crops with horizontal canopies that completely cover the soil [24]. The model's general expression for partitioning the available radiation ($R_n - G$, where R_n is the net solar radiation and G is the soil heat flux) into latent heat flux (LE) and sensible heat flux (H) can be written as proposed by Shuttleworth and Wallace [20] in the following form (Equation (1)):

$$R_n - G = H + LE \quad (1)$$

However, it is crucial to assess the energy partitioning between canopy and soil in sparse crops planted in rows, where a significant fraction of the soil remains exposed under and between the crop rows [12,14,15,18,24].

Net radiation fluctuations are influenced by factors such as vine row orientation, row spacing, canopy height, the Earth's daily and seasonal rotational and orbital movements, and cloud cover intensity and duration [25]. These fluctuations impact net radiation at the vine canopy top, the soil beneath the vine canopy, and the soil between rows, varying throughout the day and season. Therefore, to better understand the divergence of available energy and derive the energy fluxes within the vineyard, this study proposes assessing the energy flux from each component—the vine canopy, bare soil between rows, and bare soil under the vines—separately. The resulting modeling framework partitions the energy balance of each soil component and the canopy, enabling the estimation of vine canopy transpiration and soil evaporation, described by Equations (2)–(4) as:

i. energy balance of vine canopy [21,24,26]:

$$R_{n,c} = H_c + LE_c \quad (2)$$

Note that, since the energy balance at the canopy level only accounts for the fluxes measured just above the canopy, the contribution of soil heat flux is negligible and can be disregarded in this calculation.

ii. energy balance under vine canopy:

$$R_{n,uc} - G_{uc} = H_{uc} + LE_{uc} \quad (3)$$

iii. energy balance between vine rows:

$$R_{n,bs} - G_{bs} = H_{bs} + LE_{bs} \quad (4)$$

For all equations, R_n is the net solar radiation (W.m^{-2}), G is the soil heat flux (W.m^{-2}), H is the sensible heat flux (W.m^{-2}), LE is the latent heat flux (W.m^{-2}). The subscripts c, uc, and bs represent the fluxes measured from the canopy, under the canopy, and above bare soil between rows, respectively.

Individual assessments of sensible and latent energy fluxes, calculated within our model framework, were used as inputs for the three-source clumped model described in Section 2.4.5. This model, initially developed by Brenner and Incoll [16] and further refined by Lhomme et al. [15], was applied to estimate the aggregated energy fluxes at a reference level above the vineyard. The aggregated fluxes derived from the three-source clumped model were then compared with energy flux measurements obtained from an eddy covariance (EC) tower installed in the experimental field.

2.4. Field and Reference Measurements

The measurement setup for calculating the turbulent energy fluxes within the proposed model framework involved the deployment of various sensors to capture key meteorological variables at different heights and locations (reference (r), canopy (c), under the canopy (uc), and bare soil between rows (bs)) within the vineyard. This section briefly describes the field measurements used to estimate the turbulent energy fluxes within the model framework and to measure the energy fluxes at the reference heights. It outlines the methods and instrumentation employed to capture the data necessary for calculating the energy fluxes within the vineyard.

All soil and meteorological sensors used were connected to a datalogger (CR1000, Campbell Scientific, Logan, UT, USA), with data collected every minute and averaged every 15 min.

2.4.1. Net Solar Radiation (R_n)

To account for energy inputs in the vineyard, net solar radiation measurements were conducted using four net radiometers (NR2, Delta-T Devices, Cambridge, UK) placed at specific locations and heights. These measurements provided the net solar radiation over the vineyard at the reference level ($R_{n,r}$), the net solar radiation above the canopy ($R_{n,c}$), the net solar radiation beneath the canopy ($R_{n,uc}$), and the net solar radiation between the vine rows ($R_{n,bs}$) data as follows:

Net Solar Radiation above the Canopy ($R_{n,c}$)

To measure the available energy above the canopy, a net radiometer was positioned at the top of the canopy, 2 m above the soil surface, and aligned with the vine canopy.

Net Solar Radiation Beneath the Canopy ($R_{n,uc}$)

To measure the available energy beneath the canopy, a net radiometer was positioned 0.3 m above soil surface, directly under the vine canopy.

Net Solar Radiation Between Vine Rows ($R_{n,bs}$)

To measure the available energy between vine rows, a net radiometer was positioned in the middle of the interrow, 0.3 m above the soil surface.

2.4.2. Soil Heat Fluxes (G)

The measurements of energy to/from the soil were conducted using two heat flux plates (HFP01, Hukseflux Thermal Sensors, Delft, The Netherlands) placed at specific locations. These measurements provided the soil heat flux beneath the canopy (G_{uc}), and the soil heat flux between vine rows (G_{bs}) data.

Soil Heat Flux Beneath the Canopy (G_{uc})

To measure the soil heat flux beneath the canopy, a heat flux plate was installed 0.05 m below the soil surface, positioned beneath the vine canopy.

Soil Heat Flux between Vine Rows (G_{bs})

To measure the soil heat flux between vine rows, a heat flux plate was installed in the middle of the interrow, 0.05 m below the soil surface.

2.4.3. Sensible Heat Fluxes (H)

The sensible heat fluxes under the canopy (H_{uc}), from the canopy (H_c), and from bare soil between rows (H_{bs}) were calculated using the soil and meteorological variables measured within the proposed model framework. The equations used to calculate the sensible heat fluxes are presented in the following sections.

Sensible Heat Fluxes under the Canopy (H_{uc})

The below-canopy sensible heat flux (H_{uc}) was computed according to Kool et al. [17] by Equation (5):

$$H_{uc} = \rho c_p \frac{T_{s,uc} - T_{a,uc}}{r_{a,uc}} \quad (5)$$

where H_{uc} is the sensible heat flux under the canopy, ρ is the air density, c_p is the air specific heat capacity at constant pressure (1013 J.kg^{-1}.°C^{-1}), $T_{s,uc}$ is the soil temperature measured beneath the canopy, $T_{a,uc}$ is the air temperature measured beneath the canopy, and $r_{a,uc}$ is the aerodynamic resistance beneath the canopy (Equation (6)).

$T_{s,uc}$ was measured using a two-junction, fine-wire copper-constantan T-type thermocouple placed approximately 0.01 m above the top surface of the G_{uc} soil heat flux sensor. In addition, $T_{a,uc}$ was recorded simultaneously with the relative humidity using a thermohygrometer (CS215-PWS Campbell Scientific, Logan, UT, USA) placed beneath the vine canopy (0.3 m above soil surface).

The aerodynamic resistance between the soil surface and the sink of the momentum below the canopy ($r_{a,uc}$) was calculated accordingly to Lhomme et al. [15] by Equation (6):

$$r_{a,uc} = \frac{h \exp(n)}{n k_h} [\exp(-n z_0'/h) - \exp(-n(z_0 + d_p)/h)] \quad (6)$$

where h is the vine canopy height (m), n is the eddy diffusivity decay coefficient (following Shuttleworth and Wallace [20], n = 2.5, dimensionless), k_h is the eddy diffusivity at the top of the canopy (m^2.s^{-1}), z_0' is the bare soil roughness length (m), equal to 0.01 m [15], z_0 is the canopy roughness length (z_0 = 0.13 h, m), and d_p is the zero-plane displacement height (d_p = 0.6 h, m).

Sensible Heat Fluxes from the Canopy (H_c)

The sensible heat fluxes from the canopy (H_c) were computed according to Kool et al. [17] by Equation (7):

$$H_c = \rho c_p \frac{T_c - T_{a,c}}{r_{a,c}} \quad (7)$$

where H_c is the sensible heat flux from the canopy, ρ is the air density, c_p is the air specific heat capacity at constant pressure (1013 J.kg^{-1}.°C^{-1}), T_c is the canopy temperature, $T_{a,c}$ is the air temperature measured above the canopy, and $r_{a,c}$ is the aerodynamic resistance above the canopy (Equation (8)).

To measure T_c, a thermal image was taken from the vine canopies using an infrared (IR) thermal camera (FLIR model C5, FLIR Systems Inc., Wilsonville, OR, USA), equipped with a 160 × 120 (19,200 pixels) IR sensor and operating in the 8 to 14 µm spectral range.

The thermal images were captured perpendicularly to the canopy at approximately 2 m, with an emissivity (ε) set at 0.96. Images were taken from both the sunlit and shadow

canopy sides, with one image per vine and five plants per canopy exposure (n = 10). The background temperature was determined by measuring the temperature of a crumpled sheet of aluminum foil placed near the canopy using an emissivity (ε) value of 1 [27]. Thermal images were analyzed using the 'Flir Thermal Studio' software version 2.0.21 (Flir Systems, Inc., Wilsonville, OR, USA), converted into csv files, and exported to Matlab R2023a (The Mathworks, Inc., Natick, MA, USA) to generate a temperature data matrix, where each cell corresponded to a pixel temperature value. The pixels were counted and recorded in an absolute frequency table based on their temperature range. To isolate canopy surface data and minimize interferences, pixels representing the background and vine trellising materials were excluded. The process of canopy surface data validation involved excluding all pixels with temperatures falling below the 10th percentile or above the 90th percentile. To facilitate calculations while integrating all the T_c values measured in each thermal image, a mean of all the validated pixel temperature values was assumed as representative of T_c.

$T_{a,c}$ was measured using a thermohygrometer (CS215-PWS Campbell Scientific, Logan, UT, USA) placed above the vine canopy (2 m above the soil surface). $r_{a,c}$ was then calculated according to Lhomme et al. [15] by the Equation (8):

$$r_{a,c} = \frac{\left[\left(\frac{n}{0.01}\right)\left(\frac{w}{u_h}\right)^{0.5}\left(1-\exp^{\left(-\frac{n}{2}\right)}\right)^{-1}\right]}{LAI} \quad (8)$$

where the wind speed at the top of the canopy (u_h, m.s^{-1}) was calculated from the wind speed measured at the reference height (z_r) by Equation (9) [15], as follows:

$$u_h = \left(\frac{u_*}{k}\right)\ln\left(\frac{h-d_p}{z_0}\right) \quad (9)$$

the wind friction velocity (u_*, m.s^{-1}) is given by Equation (10):

$$u_* = \frac{(ku_r)}{\ln\left[\frac{(z_r-d_p)}{z_0}\right]} \quad (10)$$

the canopy roughness length (z_0, m) is given by Equation (11) [15]:

$$z_0 = 0.13\,h \quad (11)$$

and the zero-plane displacement height (d_p, m) is given by Equation (12) [15]:

$$d_p = 0.63\,h \quad (12)$$

In the previous equations, LAI is the leaf area index (m^2.m^{-2}), z_0' is the bare soil roughness length (m), z_r is the reference height (3 m in the present study), k is the von Karman's constant (k = 0.41, dimensionless), u_r represents the wind speed at the reference height, measured with a 3D sonic anemometer (Gill Windmaster Pro, Gill Instruments Limited, Hampshire, UK) (m.s^{-1}), h is the vine canopy height (m), n is the eddy diffusivity decay coefficient (following Shuttleworth and Wallace [20], n = 2.5, dimensionless), and w is the average width of a representative leaf (m).

The average leaf width, w, was measured from 20 leaves (two median-sized leaves from each of the 10 grapevines selected for the research), resulting in an estimated mean of 0.18 m. The leaf area index (LAI) of the grapevines was determined using a non-destructive allometric method applied to the same 10 selected grapevines. The total leaf area was computed using the method described by Lopes and Pinto [28]. Subsequently, LAI was estimated by dividing the total leaf area by the area occupied by each individual vine. The surface area of each vine was calculated by considering the space between vines and the

projection of the canopy shadow at midday. Since the distance between vines is fixed and the canopy maintains a consistent shape, the surface area is estimated by multiplying the fixed distance between the vines by the horizontal distance of the canopy shadow projected at midday. This procedure ensures an accurate representation of the spatial area occupied by each vine within the row, with minimal overlap between adjacent vines. Measurements were conducted on four separate occasions: 14 July 2021, 16 August 2021, 17 August 2021, and 24 August 2021. The measured *LAI* values for the selected vines consistently fell within the range of 1.8 to 2.1 $m^2.m^{-2}$ throughout the experimental period; therefore, a mean value of 2.0 $m^2.m^{-2}$ was employed in the analysis.

Sensible Heat Fluxes from Bare Soil Between Rows (H_{bs})

Variations in the sensible heat fluxes between rows (H_{bs}), were accounted for as a difference in temperatures across the bare soil and air resistances [29], as described by Equation (13):

$$H_{bs} = \rho c_p \frac{T_{s,bs} - T_{a,bs}}{r_{a,bs}} \quad (13)$$

Equation (13) represents the computation of the bare soil heat flux (H_{bs}) using the soil surface temperature ($T_{s,bs}$), air temperature ($T_{a,bs}$), and the aerodynamic resistance above bare soil between rows ($r_{a,bs}$). Additionally, ρ represents the air density, and c_p represents the specific heat capacity of air at constant pressure (1013 $J.kg^{-1}.^{\circ}C^{-1}$).

The $T_{s,bs}$ was measured using a two-junction, fine-wire copper-constantan T-type thermocouple placed approximately 0.01 m above the top surface of the G_{bs} soil heat flux sensor. The $T_{a,bs}$ was measured simultaneously with the relative humidity using a thermohygrometer (CS215-PWS Campbell Scientific, Logan, UT, USA) placed in the middle of the interrow (0.3 m above soil surface).

The $r_{a,bs}$ was calculated according to Brenner and Incoll [16] by the Equation (14):

$$r_{a,bs} = \frac{\ln\left(\frac{z_m}{z_0'}\right)^2}{(k^2 u_m)} \quad (14)$$

where z_m represents the mean surface flow height [16]. In the present study, the mean surface flow height between vine rows was assumed to be 0.30 m. The z_0' represents the bare soil roughness length (m), equal to 0.01 m [15], k denotes the von Karman's constant (k = 0.41, dimensionless), and u_m stands for the wind speed at the mean surface flow height ($m.s^{-1}$).

Wind speed measurements were obtained using a 2D sonic anemometer (Gill Ultrasonic ANE 5M, Gill Instruments Limited, Hampshire, UK) positioned 0.3 m above the soil surface, between vine rows, and facing the predominant north winds.

2.4.4. Latent Heat Fluxes Estimation

In the present model framework, the latent heat fluxes were calculated as the unknowns of Equations (2)–(4) by:

i. The latent heat above the canopy (LE_c) [21,24,26]:

$$LE_c = R_{n,c} - H_c \quad (15)$$

ii. The latent heat from soil beneath the canopy (LE_{uc}):

$$LE_{uc} = R_{n,uc} - G_{uc} - H_{uc} \quad (16)$$

iii. The latent heat from bare soil between vine rows (LE_{bs}):

$$LE_{bs} = R_{n,bs} - G_{bs} - H_{bs} \quad (17)$$

2.4.5. Estimation of Energy Fluxes at the Reference Level

To validate the accuracy of the fluxes calculated from each component (soil and canopy) within the proposed model framework (using Equations (5), (7), (13), (15), (16), and (17)), these turbulent fluxes were aggregated at a reference height above the vineyard. The calculated fluxes for each component within the proposed model framework were used as inputs for a three-source clumped model, originally formulated by Brenner and Incoll [16] and further developed by Lhomme et al. [15], to calculate the energy fluxes at the reference height. The formalism concerning the calculation of total resistances and fluxes over heterogeneous and sparse canopies used in this work is explained in detail in Lhomme et al. [15].

Estimated Sensible Heat Flux at the Reference Level

Figure 2 illustrates a visual representation of the modeling framework for sensible heat fluxes (H) and the depiction of air and surface temperatures originating from a sparse canopy. Within this model framework, the aggregation of sensible heat fluxes at the reference height (z_r) is given by Equation (18) [16]:

$$H_r = f(H_{uc} + H_c) + (1 - f)H_{bs} \quad (18)$$

where H represents the sensible heat flux (W.m^{-2}), and f is the fractional cover of the canopy (0.3 under present conditions), representing the area of soil covered by the projected canopy shade at midday. The subscripts r, uc, c, and bs represent the fluxes estimated at specific locations relative to the canopy and soil surfaces: at the reference height (at the EC system height), under the canopy (from bare soil surface to the base of the canopy), immediately above the canopy, and above bare soil surface between rows, respectively.

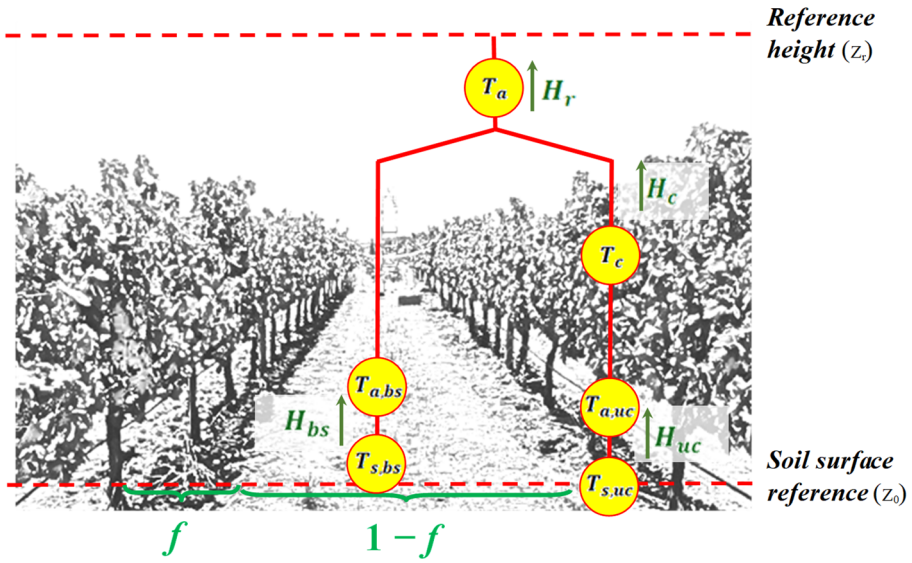

Figure 2. Schematic representation of the three-source clumped model for convective fluxes (specifically sensible heat, H) partitioning in a sparse canopy, illustrating the associated air and surface temperatures.

Estimated Latent Heat Flux at the Reference Level

Similarly, within the presented modeling framework, the aggregated latent heat fluxes (LE) at the reference height (z_r) are given by Equation (19) [16]:

$$LE_r = f(LE_{uc} + LE_c) + (1 - f)LE_{bs} \quad (19)$$

This equation describes the estimated latent heat flux (LE_r) at the reference height, where LE_{uc}, LE_c, and LE_{bs} represent latent heat fluxes calculated from Equations (15) to (17) for the regions under the canopy, from the canopy, and above the bare soil between rows, respectively. As with the sensible heat fluxes, f represents the fractional cover of the canopy.

2.4.6. Energy Fluxes Measured at the Reference Level

To validate the estimated fluxes aggregated at the reference heights, LE_r and H_r, an eddy-covariance (EC) system was installed on the experimental plot. This system enabled the measurement of the vertical profile of energy fluxes, including the observed latent heat flux (LE_{obs}) and sensible heat flux (H_{obs}) at the reference level (z_r), over the experimental vineyard.

The EC system comprised a 3D sonic anemometer (Gill Windmaster Pro, Gill Instruments Limited, Hampshire, UK) oriented to a fast-response, 0.1 Hz, open-path CO2/H2O analyzer (LI-6500 DS, LI-COR Inc., Lincoln, NE, USA) and connected to a Smartflux 3 system (LI-COR Inc., Lincoln, NE, USA). Both the sonic anemometer and the open-path CO2/H2O analyzer were positioned at a height of 3.0 m above the ground surface, directly over the canopy top, and oriented towards the predominant north winds. The EC system facilitated high-temporal-resolution recording of monitored reference latent heat (LE_{obs}) and sensible heat (H_{obs}) fluxes at intervals of every 1/10 s.

Net Solar Radiation over the Vineyard, at the Reference Level

To measure the available energy above the vineyard, at the reference level (Rn_{obs}), a net radiometer was positioned at a height of 3 m.

Reference Soil Heat Flux

The reference soil heat flux was assessed using six heat flux plates (Hukseflux HFP01, Hukseflux Thermal Sensors, Delft, The Netherlands) placed at a depth of 0.05 m. One plate was positioned beneath the vine canopy within the row (also used to measure G_{uc}), while the remaining plates were evenly spaced at 0.5 m intervals perpendicular to the vine rows, covering the entire interrow area. To calculate the reference soil heat flux (G_{obs}) between vine rows, it was necessary to account for the coexisting differences between shaded and exposed soil areas. Therefore, the G_{obs} value was calculated as the average of the measured heat flux at each point along the interrow cross-section.

Overall Assessment of the Balance Fluxes at the Reference Level

Data quality assessment and analysis were conducted using EddyPro software v7.0.6 (LI-COR Inc., Lincoln, NE, USA). The measurement site was situated within a larger vineyard of the same variety and subjected to identical viticultural practices, ensuring a homogenous fetch. A minimum fetch of 300 m, encompassing the experimental field, was maintained to ensure that all fluxes within the area of interest were captured, thereby minimizing the influence of advective fluxes from surrounding areas. A linear regression analysis was performed between the turbulent energy fluxes (LE_{obs} + H_{obs}) and the available energy (solar radiation, Rn_{obs}, and soil heat flux, G_{obs}), using 15-min averaged measurements throughout the study period. This analysis revealed that more than 90% of the analyzed fluxes achieved an energy balance closure of approximately 0.95 (Figure 3). Similar energy balance closure results have been reported in previous studies [17,30–33]. Table 2 provides a summary of the reference field measurements and the instrumentation employed.

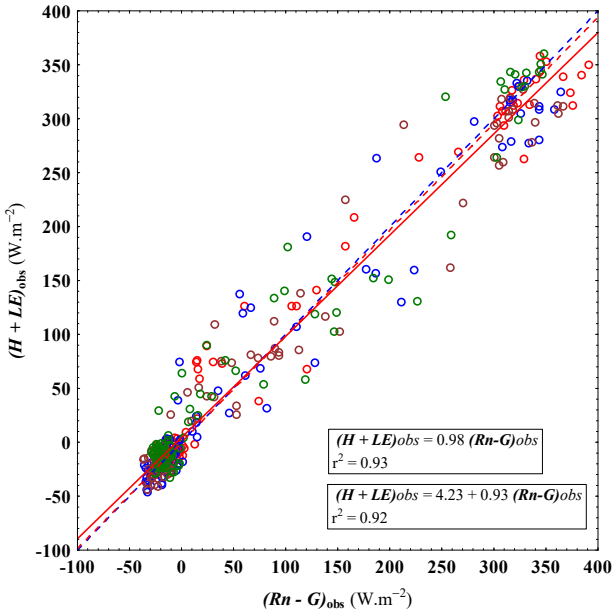

Figure 3. Least squares linear regression (solid red line) between the observed turbulent energy fluxes $(H + LE)_{\text{obs}}$ and the available energy $(Rn - G)_{\text{obs}}$, both measured at the reference level. The colored circles represent data collected on specific dates: 15 July (red), 10 August (blue), 18 August (brown), and 26 August (green). The dashed red line represents the least squares linear regression forced through the origin (y = ax), where *a* is the slope indicating the proportionality between turbulent energy fluxes and available energy. The dashed blue line corresponds to the 1:1 relationship (y = x), signifying a perfect match between the turbulent energy fluxes and available energy.

Table 2. Summary of variables used for measuring the validation set of energy fluxes: field measurements and instrumentation.

Variable	Periodicity and Data Integration	Units	Source
Net radiation (Rn_{obs})	Every minute and averaged every 15 min	$W.m^{-2}$	Net radiometer, model NR2, (Delta-T Devices, Cambridge, UK)
Soil heat flux (G_{obs})			Hukseflux sensor (model HFP01, Hukseflux Thermal Sensors, Delft, The Netherlands)
Wind speed (u_{obs})	Every 1/10 s and averaged every 15 min	$m.s^{-1}$	3D sonic anemometer (model Gill Windmaster Pro, Gill Instruments Limited, Hampshire, UK)
Latent heat (LE_{obs})		$W.m^{-2}$	EC system comprised by a fast-response, 0.1 Hz, open-path CO2/H2O analyzer (LI-6500 DS, LI-COR Inc., Lincoln, NE, USA)
Sensible heat (H_{obs})			

2.5. Evaluation of the Estimated Energy Fluxes at the Reference Height

The energy fluxes estimated at the reference height, H_r and LE_r, were validated by comparison with the energy fluxes measured by the EC system at the same reference height. The validation process involved fitting the estimated energy flux values (e^i_Φ) calculated by Equations (18) and (19) to the observed energy fluxes (o^i_Φ) measured by the EC system. This evaluation included both convective energy fluxes (Φ), which encompassed the latent energy flux (LE), and sensible energy fluxes (H).

The model's performance was assessed using several statistical parameters, including Pearson's coefficient of correlation (R), root-mean-square error ($RMSE$), mean bias error (MBE), and relative error ($|E|$). These parameters are defined as follows:

$$RMSE = \sqrt{\frac{\sum_{i=1}^{n}\left(e^i_\Phi - o^i_\Phi\right)^2}{n}} \quad (20)$$

$$MBE = \frac{\sum_{i=1}^{n} \left(e_{\Phi}^{i} - o_{\Phi}^{i} \right)}{n} \quad (21)$$

$$|E| = \frac{\left| \sum_{i=1}^{n} \left(e_{\Phi}^{i} - o_{\Phi}^{i} \right) \right|}{\sum_{i=1}^{n} o_{\Phi}^{i}} \times 100 \quad (22)$$

In these formulas, e_{Φ}^{i} represents the i-th value of the energy flux estimated by the three-source clumped model formulated in Equations (18) and (19) from a dataset of n = 320 elements. Similarly, o_{Φ}^{i} denotes the i-th observed value of energy flux measured by the EC system during the same period. Here, the subscript Φ stands for the convective energy fluxes, encompassing both latent energy flux (*LE*) and sensible heat flux (*H*).

Model evaluation processes were implemented using Matlab R2023a (The Mathworks Inc., Natick, MA, USA).

3. Results and Discussion

3.1. Characterization of the Available Energy and Turbulent Energy Fluxes Within the Proposed Model Framework

The daily and seasonal variation of the sun's apparent movement, combined with the orientation of vine rows and the structure and dimensions of the canopy, differentially affected the shadow cast by the vine canopy. This variation influenced the extension of exposed canopy and soil areas, as well as the intensity of incident radiation within the vineyard. Consequently, the available energy at various points in the vineyard fluctuated throughout the day and season.

In this section, we analyze and discuss the variability of the available energy and how it was partitioned into sensible and latent heat fluxes throughout our experiment. Conventionally, the net radiation energy flux terms (R_n and G) used here are considered positive when directed towards the surface and into the soil, while the turbulent fluxes (H and LE) are positive when directed away from the surface.

3.1.1. Available Energy Within the Model Framework

In the present experiment, the available energy at the top of the canopy ($R_{n,c}$) followed a consistent pattern across all measurement days, increasing from sunrise to a peak at 2 pm and decreasing thereafter (Figure 4a). The daily variation patterns of available energy beneath the canopy ($(R_n - G)_{uc}$) also remained consistent across the measurement days (Figure 4b), as was the energy available between the vine rows $(R_n - G)_{bs}$ (Figure 4c).

At the beginning and end of the day, the available energy between vine rows was minimal, reaching its maximum when the space between rows was fully or almost fully exposed to sunlight (Figure 4c). In contrast, the available energy beneath the canopy was highest at the beginning and end of the day, peaking at approximately 350 to 380 W.m^{-2} around 12 am and 4 pm, when the shadow projected by the vine canopy over the row was minimal. Between 12 am and 4 pm, the shadow projected by the canopy reduced the net radiation at the soil beneath the canopy to zero, thus resulting in negative available energy beneath the canopy (Figure 4b); similar results were described by Kool et al. [17]. A rapid transition occurs between the maximum values of $(R_n - G)_{uc}$ and $(R_n - G)_{bs}$ at noon and 4 pm. Additionally, the available energy beneath the canopy was influenced by irrigation, which impacted the soil's heat flux (G) and the distribution of energy under the canopy. The results indicate that G_{uc} on 10 and 26 August was slightly lower than that observed on the days before irrigation, leading to a slight decrease in the available energy beneath the canopy when topsoil water content was higher (Figures 4b and S2); comparable results were found by Heitman et al. [34].

Throughout the clear measurement days, the available energy at the canopy level was predominantly influenced by the optical properties of the leaves, particularly their albedo, accounting for approximately 72% of the available energy. This aligns with findings reported by Pieri and Gaudillère [35], who observed similar values in their studies.

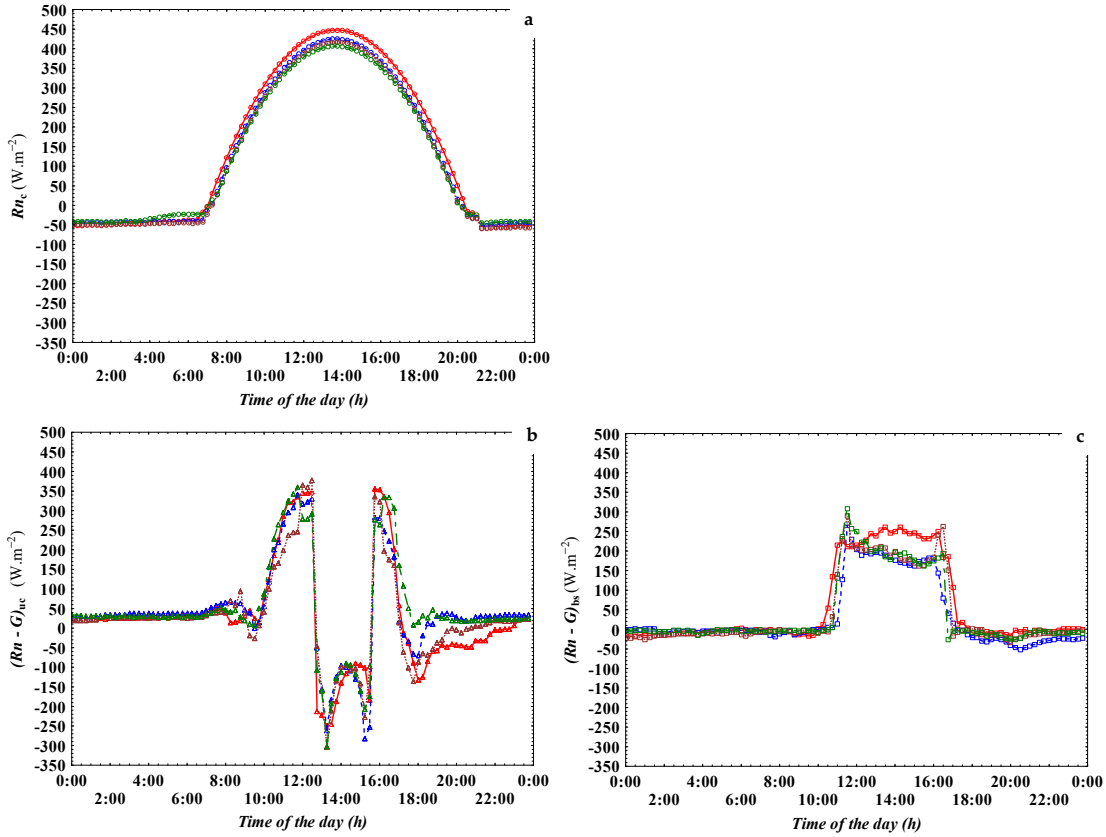

Figure 4. Energy available to each component within the proposed model framework. (**a**) Shows the net radiation measured above the canopy ($R_{n,c}$), (**b**) shows the available energy measured under the canopy ($R_{n,uc} - G_{uc}$), and (**c**) shows the available energy measured between vine rows ($R_{n,bs} - G_{bs}$), where $R_{n,i}$ and G_i are the net solar radiation and the soil heat flux measured in the i-th compartment, respectively. The solid red line represents the data measured on 15 July, the blue dashed line the data measured on 10 August, the brown dotted line the data measured on 18 August, and the green dash-dotted line the data measured on 26 August.

3.1.2. Turbulent Fluxes Within the Model Framework

Available radiation at the soil surface and soil water content significantly influenced the partition of turbulent fluxes (H and LE) throughout the experiment. As the time since the last irrigation increased, the soil under the vine canopy dried out, reducing the evaporative cooling effect and leading to an increase in measured soil temperature. The measured canopy temperature followed a similar pattern. As soil water content diminished (Figure S2), vine canopy resistance increased, causing a rise in canopy temperatures due to reduced heat dissipation through transpiration. Indeed, a higher H_c was measured on 15 July and 18 August (four and five days after last irrigation, respectively) compared to 10 and 26 August (two days after irrigation or during ongoing irrigation) (Figure 5a).

As time elapsed since the last irrigation, H_c progressively increased. This resulted from the lower vine transpiration rates and consequent reduction in evaporative cooling (with latent heat representing approximately 20% of the total available energy). Consequently, H_c reached 70% and 72% of the available energy at the canopy surface on 15 July and 18 August, respectively (Figures 4a and 5a). Additionally, on those same days, the available energy beneath the canopy was entirely converted into sensible energy fluxes (H_{uc}) (Figures 4b and 5b). On 26 August, with irrigation ongoing, H_c decreased throughout the day, accounting for approximately 50% of the energy available at the canopy level. On 10 August, just two days after irrigation, H_c accounted for an average of 65% of the total available energy at the canopy surface, remaining consistent throughout both the morning (from 9 am to 12 pm) and the afternoon (from 4 pm to 7 pm) (Figures 4a and 5a). Meanwhile,

beneath the canopy, H_{uc} accounted for an average of 60% and 50% of the total available energy beneath the canopy on the 10 and 26 of August, respectively (Figures 4b and 5b).

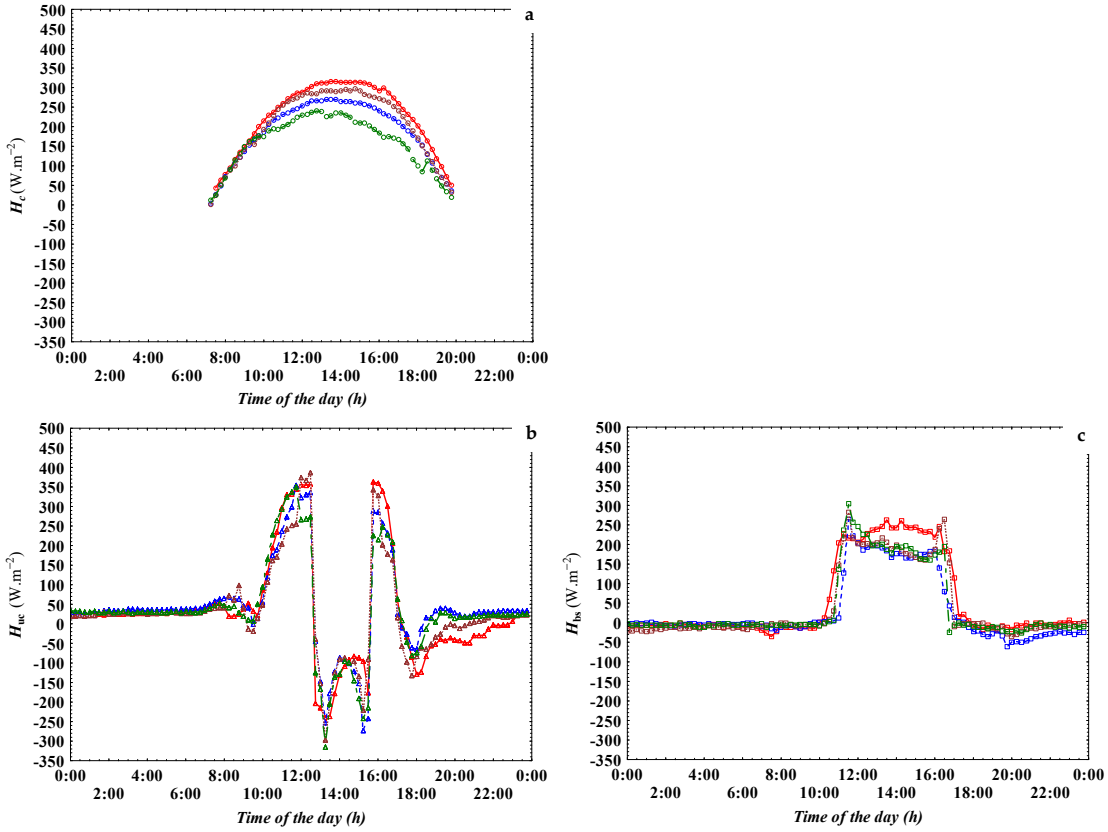

Figure 5. Estimated sensible heat fluxes from each component within the proposed model framework. (**a**) Shows the sensible heat above the canopy (H_c) calculated by Equation (7), (**b**) shows the sensible heat under the canopy (H_{uc}) calculated by Equation (5), and (**c**) shows the sensible heat between vines row (H_{bs}) calculated by Equation (13). The solid red line represents the data measured on 15 July, the blue dashed line the data measured on 10 August, the brown dotted line the data measured on 18 August, and the green dash-dotted line the data measured on 26 August.

Low soil water content, particularly surface dryness, significantly influenced the estimated sensible heat fluxes from both the soil beneath the canopy (H_{uc}) (Figure 5b) and from the canopy itself (H_c) (Figure 5a). With low soil water content, the available energy was primarily allocated to surface heating processes, as minimal evaporative cooling occurred due to the lack of soil moisture (Figure S2). In contrast, during the days following irrigation, such as 10 and 26 August, the energy was diverted towards soil water evaporation (Figure 6b), resulting in lower sensible heat fluxes from both H_{uc} and H_c (Figure 5a,b). Maximum values of 316 and 298 W.m^{-2} were calculated for H_c on 15 July (four days after irrigation) and 18 August (five days after irrigation), respectively. In contrast, maximum values of 270 and 240 W.m^{-2} were calculated for H_c on 10 August (two days after irrigation) and 26 August (irrigation ongoing), respectively (Figure 5a). Furthermore, a higher amplitude between the maximum and minimum estimated values of H_c was observed when soil water content was lower. This indicates a diminished ability of the canopy to dissipate heat through transpiration, which in turn led to greater fluctuations in sensible heat flux. As observed by Hsu and Dirmeyer [36], the present data also suggest that the higher soil moisture content, both in the topsoil layer and in the deeper soil profile where the roots extract water, can contribute to moderating soil and vine canopy temperatures. This results in lower sensible heat fluxes calculated from both the soil under the canopy and the canopy itself.

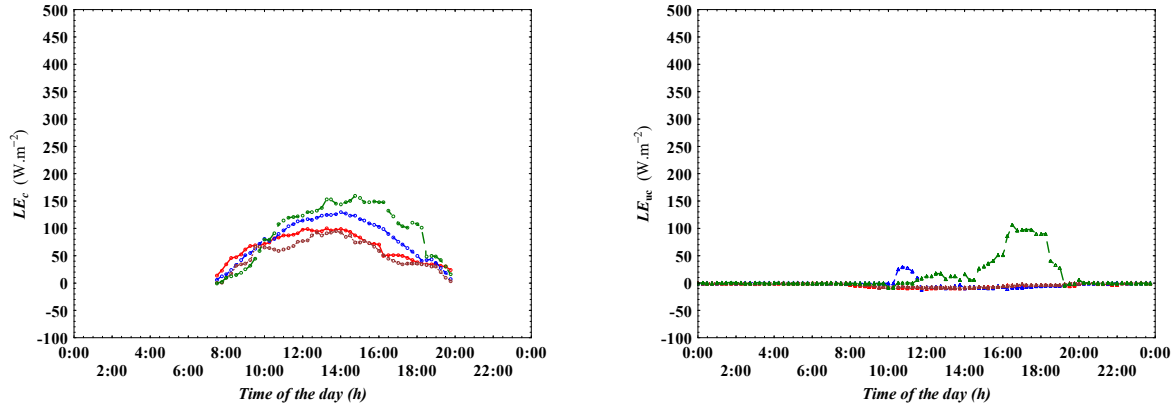

Figure 6. Estimated latent heat fluxes from each component within the proposed model framework. (**a**) Shows the latent heat calculated above the canopy (LE_c), and (**b**) shows the latent heat calculated under the canopy (LE_{uc}). The solid red line represents the data measured on 15 July, the blue dashed line the data measured on 10 August, the brown dotted line the data measured on 18 August, and the green dash-dotted line the data measured on 26 August.

Due to the characteristics of vine drip irrigation and the absence of precipitation, the soil between vine rows remained dry throughout the experimental period. Consequently, all the energy available at the soil surface between vine rows was converted into sensible heat fluxes (H_{bs}). The fluctuations of H_{bs} during the day were solely influenced by the canopy's shadow projection on the soil between vine rows (Figure 5c).

Maximum values of 29 and 107 W.m^{-2} were estimated for LE_{uc} on 10 August (two days after irrigation) and 26 August (with irrigation ongoing), respectively (Figure 6b). On 26 August, the estimated LE_{uc} values represented approximately 40% of the estimated turbulent fluxes beneath the canopy $(H+LE)_{uc}$ (Figure 6a,b). In contrast, the contribution of LE_{uc} to the total fluxes on 10 August was almost negligible (Figure 6b). Near-zero values for LE_{uc} were estimated on days when the topsoil was dry, such as 15 July and 18 August (Figure 6b). Similarly, the latent heat fluxes from the canopy (LE_c) were significantly influenced by irrigation. Increased soil moisture reduced canopy resistance, leading to higher LE_c values on 10 August and particularly on 26 August (Figure 6a). On these days, LE_c accounted for approximately 30 to 40% of the estimated turbulent fluxes from the canopy $(H+LE)_c$ (Figure 6a,b).

3.2. Model Performance Evaluation

3.2.1. Turbulent Energy Fluxes at Reference Level

To accommodate the dynamics of vineyard systems and capture all turbulent energy fluxes—encompassing those from the bare soil between rows, the bare soil beneath the canopy, and the vine canopy—a tailored energy balance model framework was proposed. This section presents a characterization of the turbulent energy fluxes estimated using a three-source clumped model at the reference level, as described by Equations (18) and (19).

It is worth noting that, during the measurement period, H_{est} accounted for approximately 65% of the available energy at the reference level on 15 July and 18 August. In contrast, on irrigation days or close to irrigation, H_{est} accounted for an average of 58% of the available energy at reference level (Table 3). This pattern, which mirrors observations at the vine canopy level, highlights the influence of soil water content, particularly due to irrigation, on the partitioning of available energy into sensible and latent heat fluxes. This is consistent with findings reported by Kool et al. [14] and Choudbury and Monteith [37].

Table 3. Proportion of the radiative energy partition between the sensible (H_{est}) and latent (LE_{est}) energy fluxes estimated at reference level. On 15 July and 18 August, data were measured under dry topsoil conditions. On 10 August data were measured two days post-irrigation and on 26 August data were measured while irrigation was ongoing.

DAY	$H_{est}/(Rn - G)_{obs}$	$LE_{est}/(Rn - G)_{obs}$
15/07/2021	0.67	0.28
10/08/2021	0.56	0.38
18/08/2021	0.66	0.26
26/08/2021	0.58	0.48

Throughout the experimental period, the estimated sensible heat flux (H_{est}) closely resembled the observed heat flux (H_{obs}), which was measured by the EC system. Although H_{est} slightly underestimated H_{obs}, the variability of H_{est} closely aligned with the observed variability in H_{obs}. Similarly, the latent heat flux (LE_{est}) estimated by the proposed model framework also showed a slight underestimation of approximately 4 W.m^{-2} compared to the observed latent heat flux (LE_{obs}) during daylight hours (Table 4). Consequently, the combined energy fluxes (H+LE) estimated by the model slightly underestimated the observed fluxes by about 5 W.m^{-2} during the same period (Table 4).

Table 4. Goodness-of-fit measures between the observed convective energy fluxes (Φ_{obs}), encompassing the latent (LE), sensible (H), and the combined (H+LE) energy fluxes, and the corresponding model-estimated fluxes (Φ_{est}) calculated using Equations (18) and (19). Observed fluxes were measured by the eddy-covariance system at the reference height (3 m). Data presented are for daylight hours only.

DAY	Energy Flux	*RMSE* (W.m^{-2})	*MBE* (W.m^{-2})	$\|E\|$ (Dimensionless)	N
15/07/2021	*H*	2.99	−0.37	0.26	50
	LE	4.46	−1.68	2.80	
	H + *LE*	10.90	−1.50	0.74	
10/08/2021	*H*	2.08	−0.03	0.03	50
	LE	5.33	−0.88	1.23	
	H + *LE*	11.10	−2.44	1.37	
18/08/2021	*H*	2.69	0.70	0.58	50
	LE	8.34	−5.76	10.77	
	H + *LE*	11.42	−5.68	3.25	
26/08/2021	*H*	2.16	−0.40	0.37	50
	LE	11.41	−8.51	8.76	
	H + *LE*	15.87	−10.94	5.31	
ALL DAYS	*H*	2.51	−0.03	0.02	200
	LE	7.87	−4.21	5.96	
	H + *LE*	12.49	−5.14	2.70	

3.2.2. Model Validation

To evaluate the ability of the proposed model framework to capture the dynamics of turbulent energy fluxes, the model-estimated fluxes at a reference level (the same height as the EC system) were validated against the fluxes observed by the EC system.

This section presents the results of the validation of the estimated sensible heat flux (by Equation (18)) and the estimated latent heat fluxes (by Equation (19)) against the respective fluxes measured by the EC system.

The validation of the energy fluxes estimated at the reference height involved fitting the estimated energy fluxes values (e^i_Φ) to the observed energy fluxes (o^i_Φ), measured by the EC system (Figure 7 and Table 4). This evaluation included both convective energy fluxes (Φ), encompassing the latent energy flux (LE), and sensible energy fluxes (H).

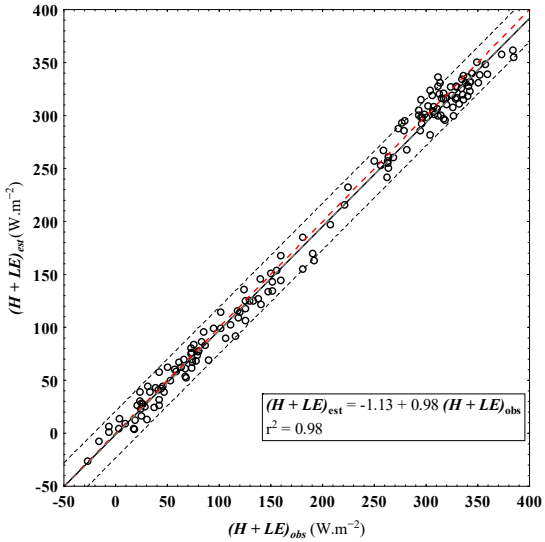

Figure 7. Least square linear regression (solid black line) between observed turbulent fluxes $(H+LE)_{obs}$, measured by the eddy-covariance system at the reference height (3 m), and the estimated turbulent fluxes $(H+LE)_{est}$, calculated using Equations (18) and (19). The black dotted lines represent the 95% confidence prediction interval, and the red dashed line indicates the 1:1 relationship (perfect agreement between observed and estimated turbulent fluxes).

Table 4 presents the accuracy measures of the proposed model framework to estimate the turbulent energy fluxes at the reference height, calculated by Equations (18) and (19). These accuracy metrics allow the assessment of the extent to which the estimated fluxes align with those measured by the EC system.

The model's estimated fluxes demonstrate a high degree of agreement with the reference fluxes measured by the EC system, as illustrated in Figure 7. The model's performance is further supported by the metrics for the deviation of the residuals, which reveal a minimal discrepancy between the observed and estimated values of the turbulent fluxes, including sensible heat flux (H), latent heat flux (LE), and the combined fluxes ($H+LE$). Notably, the average error magnitude between the observed and estimated sensible heat fluxes was consistently lower than 3 W.m^{-2} (Table 4). While the model slightly underestimated the sensible heat fluxes at the reference level, the deviation was minimal, indicating strong model performance. Similarly, latent energy fluxes were underestimated during the experimental period, with a particularly noticeable deviation on 26 August, when irrigation was ongoing. On this date, the mean bias between the estimated and observed LE was -8.5 W.m^{-2}, suggesting that while the model performed well overall, it tended to underpredict latent heat flux under conditions of increasing soil moisture due to irrigation (Table 4). Similar findings were reported by Poblete-Echeverria and Ortega-Farias [32]. It is important to emphasize that all goodness-of-fit metrics underscore the model's robustness within the specific conditions of this study. These metrics indicate that the model reliably estimated the energy fluxes in vineyard systems, despite slight underestimations that occurred under certain irrigation conditions. The high degree of agreement between the observed and estimated fluxes reaffirms the model's accuracy in capturing the complex dynamics of energy fluxes in viticultural environments. This validation of the energy fluxes estimated from each component—both soil and canopy—within the proposed model framework underscores the model's effectiveness in accurately reflecting the intricate energy dynamics at play in vineyard systems.

4. Conclusions

The water content in the soil plays a crucial role not only in regulating the temperature of the soil beneath the canopy but also in influencing the temperature and energy balance of the canopy itself. This study reveals that, even when vines are maintained under moderate

water stress, the application of controlled volumes of water can significantly alter the energy fluxes in both the canopy and the soil beneath it, particularly under conditions of intense heat stress. Given that grape clusters are typically located in the lower part of the canopy, these findings underscore the potential of irrigation management to mitigate heat stress at the level of the vine bunches.

By treating the under-canopy fluxes separately, the three-source model enables the estimation of soil evaporation under the canopy—affected by shading—and vine transpiration. This distinction is important for water resource management, particularly in vineyards employing regulated deficit irrigation, where water use efficiency is a primary concern. The three-source model separately estimates the sensible heat fluxes from both the soil beneath the canopy (H_{uc}) and the canopy (H_c) itself. This separation is important because these fluxes can differ in magnitude and behavior due to the effects of canopy shading and microclimatic variations. In vineyard systems, characterized by spatially discontinuous canopies and distinct rows, the three-source model provides a more realistic description of the energy dynamics by addressing the fluxes from both the vine canopy and the underlying soil.

This research demonstrates the feasibility of evaluating the energy fluxes within a model framework that accounts for variations in energy fluxes beneath the vine canopy, from the canopy itself, and from the bare soil between vine rows. Furthermore, it underscores the importance of accurately estimating the energy fluxes at different key vineyard locations. By enhancing our understanding of energy dynamics in vineyard ecosystems under regulated deficit irrigation, this study emphasizes the critical role of thermal and water stresses in controlling these fluxes. These insights are crucial for optimizing irrigation management practices, ultimately improving grape production in arid climates. Effective irrigation strategies can enhance both grape quality and yield while ensuring sustainability in challenging environments.

To further refine and optimize the control of heat stress in vineyards, additional research is warranted. Future studies should investigate a range of factors at both the plant and soil levels, including different planting row distances, vine row orientations, pruning techniques, and trellis systems. Additionally, exploring various soil coverings, such as cover crops or mulching, and irrigation management and applied water volumes, will provide a more comprehensive understanding of the dynamics associated with energy fluxes in vineyard systems. This holistic approach will help develop improved practices for protecting grape quality and vineyard health under varying environmental conditions.

Supplementary Materials: The following supporting information can be downloaded at: https://www.mdpi.com/article/10.3390/agriculture14101845/s1, Figure S1: Rainfall and irrigation events recorded from 15 June to 15 September 2021, in the experimental vineyard. The figure displays periods of irrigation (marked by vertical lines) and the last recorded rain event (17 June to 20 June), highlighting the dry conditions leading up to the measurements; Figure S2: Soil water content (SWC): (a) measured at the soil surface layer (0.1 m) using an ML3 Thetaprobe sensor (Delta-T Devices, Cambridge, UK), and (b) measured at 0.2 m, 0.6 m, and 0.8 m depths, with daily maximum values recorded during the measurement events on 15 July (red line), and 10 August (blue line), 18 (brown line), and 26 (green line) using an Enviroscan probe (Sentek Sensor Technologies, SA, Australia). Table S1: Adapted and measured parameters, and measured and calculated variables; Table S2: Characterization of the Canopy temperature (Tc) and Air temperature beneath the canopy (Ta,uc) on the measurement days, 15 July, 10, 18 and 26 of August 2021.

Author Contributions: Conceptualization, R.E.; methodology, R.E.; formal analysis, R.E.; investigation, R.E.; resources, A.A. and J.M.A.; data curation, R.E.; writing—original draft preparation, R.E.; writing—review and editing, R.E., A.A. and J.M.A.; supervision, A.A. and J.M.A. All authors have read and agreed to the published version of the manuscript.

Funding: This research received no external funding.

Institutional Review Board Statement: Not applicable.

Data Availability Statement: Data is available on request. The data presented in this study are available on request from the corresponding author.

Acknowledgments: We acknowledge the support of the CITES research unit, Centro de Investigación en Tecnología, Energía y Sostenibilidad, Universidad de Huelva and the FCT Research Unit "GREEN-IT -Bioresources for Sustainability" (UIDB/04551/2020—DOI 10.54499/UIDB/04551/2020, and UIDP/04551/2020—DOI 10.54499/UIDP/04551/2020). We also address our acknowledgements to Herdade do Esporão (Reguengos de Monsaraz, Alentejo, PT) and Rui Flores for their contribution to field management of the experimental vineyard.

Conflicts of Interest: The authors declare no conflicts of interest.

List of Symbols

Energy flux variables

$R_{n,c}$	Net solar radiation at the top of vine canopy (W.m^{-2})
$R_{n,uc}$	Net solar radiation under vine canopy (W.m^{-2})
$R_{n,bs}$	Net solar radiation between vine rows (W.m^{-2})
$R_{n,obs}$	Net solar radiation measured at the reference height (W.m^{-2})
G_{uc}	Soil heat flux under vine canopy (W.m^{-2})
G_{bs}	Soil heat flux between vine rows (W.m^{-2})
G_{obs}	Soil heat flux measured at the reference height (W.m^{-2})
H	Sensible heat flux (W.m^{-2})
H_c	Sensible heat flux from vine canopy (W.m^{-2})
H_{uc}	Sensible heat flux under vine canopy (W.m^{-2})
H_{bs}	Sensible heat flux between vine rows (W.m^{-2})
H_{obs}	Sensible heat flux measured at the reference height (W.m^{-2})
H_r	Sensible heat fluxes aggregated at the reference height (W.m^{-2})
LE	Latent heat flux (W.m^{-2})
LE_c	Latent heat flux from vine canopy (W.m^{-2})
lLE_{uc}	Latent heat flux under vine canopy (W.m^{-2})
lLE_{bs}	Latent heat flux between vine rows (W.m^{-2})
lLE_{obs}	Latent heat flux measured at the reference height (W.m^{-2})
lLE_r	Latent heat fluxes aggregated at the reference height (W.m^{-2})

Surface and meteorological scalar constants and variables

C_p	Air specific heat capacity at constant pressure (1013 J.kg^{-1}.°C^{-1})
d_p	Zero-plane displacement height (m)
f	Fractional cover of the canopy (dimensionless)
h	Canopy height (m)
k	Von Karman's constant (0.41 dimensionless)
k_h	Diffusivity at the top of the canopy (m^2.s^{-1})
n	Eddy diffusivity decay coefficient (2.5 dimensionless) [20]
Rn	Net solar radiation (W.m^{-2})
G	Soil heat flux (W.m^{-2})
RH	Relative humidity (%)
T_{air}	Air temperature (°C)
T_c	Canopy temperature (°C)
$T_{a,bs}$	Air temperature between vine rows (°C)
$T_{a,c}$	Air temperature above the canopy (°C)
$T_{a,uc}$	Air temperature under vine canopy (°C)
$T_{s,uc}$	Soil temperature under vine canopy (°C)
$T_{s,bs}$	Soil temperature between rows (°C)
u	Wind speed (m.s^{-1})
u_m	Wind speed at the mean surface flow height (m.s^{-1})
lu_h	Wind speed at the top of the canopy (m.s^{-1})

u_r	Wind speed measured at the reference height (m.s^{-1})
u_*	Wind friction velocity (m.s^{-1})
VPD	Vapor pressure deficit (kPa)
w	Average width of a representative leaf (m)
z_0	Canopy roughness length (m)
z'_0	Bare soil roughness length (m)
z_m	Mean surface flow height (m)
z_r	Reference height (m)
ρ	Air density (kg.m^{-3})
LAI	Leaf area index (m^2.m^{-2})
Aerodynamic resistance network	
$r_{a,bs}$	Aerodynamic resistance of bare soil unaffected by the canopy (s.m^{-1})
$r_{a,c}$	Aerodynamic resistance above the canopy (s.m^{-1})
$r_{a,uc}$	Aerodynamic resistance between bare soil under the vines canopy and z_m (s.m^{-1})

References

1. Deitch, M.J.; Sapundjieff, M.J.; Feirer, S.T. Characterizing Precipitation Variability and Trends in the World's Mediterranean-Climate Areas. *Water* **2017**, *9*, 259. [CrossRef]
2. Lionello, P.; Malanotte-Rizzoli, P.; Boscolo, R.; Alpert, P.; Artale, V.; Li, L.; Luterbacher, J.; May, W.; Trigo, R.; Tsimplis, M.; et al. The Mediterranean climate: An overview of the main characteristics and issues. *Dev. Earth Environ. Sci.* **2006**, *4*, 1–26. [CrossRef]
3. Smart, R.; Robinson, M. *Sunlight into Wine: A Handbook for Wine Grape Canopy Arrangement*; Winetitles Media: Broadview, Australia, 1991; ISBN 978-1875130108.
4. Costa, J.M.; Egipto, R.; Aguiar, F.C.; Marques, P.; Nogales, A.; Madeira, M. The role of soil temperature in mediterranean vineyards in a climate change context. *Front. Plant Sci.* **2023**, *14*, 2023. [CrossRef] [PubMed]
5. Venios, X.; Korkas, E.; Nisiotou, A.; Banilas, G. Grapevine Responses to Heat Stress and Global Warming. *Plants* **2020**, *9*, 1754. [CrossRef]
6. Del-Castillo-Alonso, M.-A.; Diago, M.P.; Tomas-Las-Heras, R.; Monforte, L.; Soriano, G.; Martínez-Abaigar, J.; Núnez-Olivera, E. Effects of ambient solar UV radiation on grapevine leaf physiology and berry phenolic composition along one entire season under Mediterranean field conditions. *Plant Physiol. Biochem.* **2016**, *104*, 379–386. [CrossRef]
7. Zarrouk, O.; Brunetti, C.; Egipto, R.; Pinheiro, C.; Genebra, T.; Gori, A.; Lopes, C.M.; Tattini, M.; Chaves, M.M. Grape Ripening Is Regulated by Deficit Irrigation/Elevated Temperatures According to Cluster Position in the Canopy. *Front. Plant Sci.* **2016**, *7*, 1640. [CrossRef] [PubMed]
8. IPCC (2019) AR6 Synthesis Report: Climate Change 2022. Available online: https://www.ipcc.ch/site/assets/uploads/2018/02/WGIIAR5-Chap3_FINAL.pdf (accessed on 30 September 2023).
9. Santillán, D.; Garrote, L.; Iglesias, A.; Sotes, V. Climate change risks and adaptation: New indicators for Mediterranean viticulture. *Mitig. Adapt. Strat. Glob. Change* **2020**, *25*, 881–899. [CrossRef]
10. Santos, J.A.; Fraga, H.; Malheiro, A.C.; Moutinho-Pereira, J.; Dinis, L.-T.; Correia, C.; Moriondo, M.; Leolini, L.; Dibari, C.; Costafreda-Aumedes, S.; et al. A Review of the Potential Climate Change Impacts and Adaptation Options for European Viticulture. *Appl. Sci.* **2020**, *10*, 3092. [CrossRef]
11. Malheiro, A.C.; Santos, J.A.; Fraga, H.; Pinto, J.G. Climate change scenarios applied to viticultural zoning in Europe. *Clim. Res.* **2010**, *43*, 163–177. [CrossRef]
12. Burchard-Levine, V.; Nieto, H.; Kustas, W.P.; Gao, F.; Alfieri, J.G.; Prueger, J.H.; Hipps, L.E.; Bambach-Ortiz, N.; McElrone, A.J.; Castro, S.J.; et al. Application of a remote-sensing three-source energy balance model to improve evapotranspiration partitioning in vineyards. *Irri. Sci.* **2022**, *40*, 593–608. [CrossRef]
13. Costa, J.M.; Egipto, R.; Sánchez-Virosta, A.; Lopes, C.M.; Chaves, M.M. Canopy and soil thermal patterns to support water and heat stress management in vineyards. *Agric. Water Manag.* **2019**, *216*, 484–496. [CrossRef]
14. Kool, D.; Ben-Gal, A.; Agam, N.; Šimunek, J.; Heitman, J.L.; Sauer, T.J.; Lazarovitch, N. Spatial and diurnal below canopy evaporation in a desert vineyard: Measurements and modeling. *Water Resour. Res.* **2014**, *50*, 7035–7049. [CrossRef]
15. Lhomme, J.P.; Montes, C.; Jacob, F.; Prévot, L. Evaporation from Heterogeneous and Sparse Canopies: On the Formulations Related to Multi-Source Representations. *Bound. Layer Meteorol.* **2012**, *144*, 243–262. [CrossRef]
16. Brenner, A.J.; Incoll, L.D. The effect of clumping and stomatal response on evaporation from sparsely vegetated shrublands. *Agric. For. Meteorol.* **1997**, *84*, 187–205. [CrossRef]
17. Kool, D.; Kustas, W.P.; Ben-Gal, A.; Lazarovitch, N.; Heitman, J.L.; Sauer, T.J. Energy and evapotranspiration partitioning in a desert vineyard. *Agric. For. Meteorol.* **2016**, *218–219*, 277–287. [CrossRef]
18. Kustas, W.P.; Alfieri, J.G.; Nieto, H.; Wilson, T.G.; Gao, F.; Anderson, M.C. Utility of the two-source energy balance (TSEB) model in vine and interrow flux partitioning over the growing season. *Irrig. Sci.* **2019**, *37*, 375–388. [CrossRef]
19. Monteith, J.L.; Unsworth, M.H. *Principles of Environmental Physics in Plants, Animals, and the Atmosphere*, 4th ed.; Academic Press: Cambridge, MA, USA, 2013; ISBN 978-0-12-386910-4.

20. Shuttleworth, J.; Wallace, J.S. Evaporation from sparse crops-an energy combination theory. *Q. J. R. Meteorol. Soc.* **1985**, *111*, 839–855. [CrossRef]
21. Norman, J.M.; Kustas, W.P.; Humes, K.S. Source approach for estimating soil and vegetation energy fluxes in observations of directional radiometric surface temperature. *Agric. For. Meteorol.* **1995**, *77*, 263–293. [CrossRef]
22. Ortega-Farías, S.; Poblete-Echeverría, C.; Brisson, N. Parameterization of a two-layer model for estimating vineyard evapotranspiration using meteorological measurements. *Agric. For. Meteorol.* **2010**, *150*, 276–286. [CrossRef]
23. Qin, S.; Fan, Y.; Li, S.; Cheng, L.; Zhang, L.; Xi, H.; Qiu, R.; Liu, P. Partitioning of available energy in canopy and soil surface in croplands with different irrigation methods. *Agric. Water Manag.* **2023**, *288*, 108475. [CrossRef]
24. Zhao, P.; Zhang, X.; Li, S.; Kang, S. Vineyard Energy Partitioning Between Canopy and Soil Surface: Dynamics and Biophysical Controls. *J. Hydrometeorol.* **2017**, *18*, 1809–1829. [CrossRef]
25. Hunter, J.K.; Tarricone, L.; Volschenk, C.; Giacalone, C.; Melo, M.S.; Zorer, R. Grapevine physiological response to row orientation-induced spatial radiation and microclimate changes. *OENO One* **2020**, *54*, 411–433. [CrossRef]
26. Ham, J.M.; Heilman, J.L. Aerodynamic and surface resistances affecting energy transport in a sparse crop. *Agric. For. Meteorol.* **1991**, *53*, 267–284. [CrossRef]
27. Jones, H.G.; Stoll, M.; Santos, T.; de Sousa, C.; Chaves, M.M.; Grant, O.M. Use of infra-red thermography for monitoring stomatal closure in the field: Application to the grapevine. *J. Exp. Bot.* **2002**, *53*, 2249–2260. [CrossRef]
28. Lopes, C.; Pinto, P.A. Easy and accurate estimation of grapevine leaf area with simple mathematical models. *Vitis J. Grapevine Res.* **2005**, *44*, 55–61. [CrossRef]
29. Shuttleworth, J.; Gurney, R.J. The theoretical relationship between foliage temperature and canopy resistance in sparse crops. *Q. J. R. Meteorol. Soc.* **1990**, *116*, 497–519. [CrossRef]
30. Fuentes, S.; Ortega-Farias, S.; Carrasco-Benevides, M.; Tongson, E.; Viejo, C.G. Actual evapotranspiration and energy balance estimation from vineyards using micro-meteorological data and machine learning modeling. *Agric. Water Manag.* **2024**, *297*, 108834. [CrossRef]
31. Kool, D.; Kustas, W.P.; Ben-Gal, A.; Agam, N. Energy partitioning between plant canopy and soil, performance of the two-source energy balance model in a vineyard. *Agric. For. Meteorol.* **2021**, *300*, 108328. [CrossRef]
32. Poblete-Echeverría, C.; Ortega-Farias, S. Estimation of actual evapotranspiration for a drip-irrigated Merlot vineyard using a three-source model. *Irrig. Sci.* **2009**, *28*, 65–78. [CrossRef]
33. Ortega-Farías, S.; Carrasco, M.; Olioso, A.; Acevedo, C.; Poblete, C. Latent heat flux over Cabernet Sauvignon vineyard using the Shuttleworth and Wallace model. *Irrig. Sci.* **2007**, *25*, 161–170. [CrossRef]
34. Heitman, J.L.; Horton, R.; Sauer, T.J.; Ren, T.S.; Xiao, X. Latent heat in soil heat flux measurements. *Agric. For. Meteorol.* **2010**, *150*, 1147–1153. [CrossRef]
35. Pieri, P.; Gaudillère, J. Sensitivity to training system parameters and soil surface albedo of solar radiation intercepted by vine rows. *Vitis* **2003**, *42*, 77–82. [CrossRef]
36. Hsu, H.; Dirmeyer, P.A. Soil moisture-evaporation coupling shifts into new gears under increasing CO_2. *Nat. Commun.* **2023**, *14*, 1162. [CrossRef] [PubMed]
37. Choudhury, B.J.; Monteith, J.L. A four-layer model for the heat budget of homogeneous land surfaces. *Q. J. R. Meteorol. Soc.* **1988**, *114*, 373–398. [CrossRef]